Available online at www.sciencedirect.com
SCIENCE DIRECT®
Journal of Photochemistry and Photobiology A: Chemistry 168 (2004) 117–132
Journal of Photochemistry and Photobiology A:Chemistry
www.elsevier.com/locate/jphotochem

New ultraviolet absorption cross-sections of BrO at atmospheric temperatures measured by time-windowing Fourier transform spectroscopy

Oliver C. Fleischmann [a], Matthias Hartmann [a], John P. Burrows [a,*], Johannes Orphal [b]

[a] *Institute of Remote Sensing, University of Bremen, 28334 Bremen, Germany*
[b] *Laboratoire de Photophysique Moléculaire, Université de Paris-Sud, F-91405 Orsay Cedex, France*

Received 30 March 2002; accepted 26 March 2004
Available online 3 July 2004

Abstract

The UV absorption cross-section spectra of the atmospherically important radical BrO have been determined using the recently developed technique of time-windowing Fourier transform spectroscopy (TW-FTS). The absorption spectra of the $A^2\Pi_{3/2}$–$X^2\Pi_{3/2}$ band system were recorded in the flash photolysis of a gaseous mixture of Br_2 and O_3. The bromine-photosensitized decomposition of O_3 was observed at five different temperatures between 203 and 298 K. The absolute UV absorption cross-section was determined from the time-dependent observation of reactant and product absorptions and by a kinetic analysis of the BrO behavior. The integrated UV absorption cross-section of BrO was, within the accuracy of the measurements, constant over the temperature range studied, as expected from spectroscopic considerations. For the (7, 0) vibrational band at 29 540 cm^{-1} (338.5 nm), the peak absorption cross-sections were determined to be 2.19 ± 0.23 at 298 K, 2.23±0.23 at 273 K, 2.52±0.26 at 243 K, 2.75±0.29 at 223 K, and 3.03±0.31 at 203 K (all in units $\times 10^{-17}$ cm^2 per molecule, at a spectral resolution of 3.8 cm^{-1}, with error intervals of 2σ). Further, vibrational constants and the dissociation limit for the electronic state $A^2\Pi_{3/2}$ were derived. The A ← X dissociation energy was determined to be $D_0 = 35\,240 \pm 160\,cm^{-1}$ or 421.6 ± 1.9 kJ/mol.

Keywords: BrO; Atmospheric remote sensing; Absorption cross-section

1. Introduction

The current importance of the BrO radical for the atmosphere can be largely attributed to its participation in catalytic cycles which destroy stratospheric and tropospheric ozone [1–5]. As a result of the photolysis of many bromine compounds in the UV and visible by solar radiation, a larger fraction of atmospheric bromine is present as BrO, compared to the fraction of atmospheric chlorine present as ClO. Similarly, the multiphase or heterogeneous activation of bromine in the stratospheric polar vortex in spring is not expected to be as significant as the activation of chlorine. The atmospheric removal of ozone by bromine reactions proceeds in the gas phase via chemical mechanisms similar to those involving chlorine reactions [4,6]. However, again as a result of the photolysis of potential bromine reservoir species, the chain length of the catalytic cycles is significantly longer for the bromine chain removal of ozone than that for chlorine.

Both in situ and remote sensing measurement techniques are being used successfully to investigate and determine the precise role of BrO in chemistry of the stratosphere and troposphere [3–5,7–11]. Anti-correlations between BrO and O_3 concentrations have been observed in the lower stratosphere. In this region, BrO is known to play a prominent role in the recycling of stratospheric Cl atoms through its reaction with ClO. This reactivation of Cl by reaction of ClO with BrO is estimated to account for 20–30% of the total O_3 loss during Antarctic spring [12,13]. The presence of bromine compounds is also known to be important in the disintegration of tropospheric ozone at high latitudes. Large clouds of BrO during an episode of low ozone have been observed by instrumentation on the ground and aboard satellites [3,5,14–18].

The determination of atmospheric BrO amounts and distributions by remote sensing measurements in the VIS/UV spectral range requires an accurate knowledge of the ab-

* Corresponding author.

1010-6030/$ – see front matter © 2004 Elsevier B.V. All rights reserved.
doi:10.1016/j.jphotochem.2004.03.026

sorption cross-sections [9,19]. These spectra are also needed for the estimation of the atmospheric photolysis rate of BrO [20,21]. Therefore, reference absorption spectra have to be recorded in laboratory measurements. The UV absorption spectrum of BrO is attributed to the electronic transition $A^2\Pi_{3/2} \leftarrow X^2\Pi_{3/2}$. The high reactivity of the BrO radical implies that it is difficult to establish large concentrations longer than a few milliseconds. For this reason, time-resolved observation methods have been employed for the determination of the absorption cross-section. In many earlier studies of BrO, homogeneous gas reactions were initiated and decay curves of the reactants were recorded by grating spectrometers employing a photomultiplier [20,22,25,26]. The concentration–time profiles were then compared to a chemical kinetics model of the experiment. Cox et al. [22] applied a modulated photolysis to gaseous samples of Br_2 and O_3. Laszlo et al. [26] used a laser pulse to photolyze Br_2/N_2O mixtures. Sander and Watson [25] and Wahner et al. [20] used a flash photolysis setup to generate BrO. Grating spectrographs have also been used in the majority of the previous studies to record the UV absorption spectrum of BrO [20,22–26]. Photomultipliers and photodiode arrays are well suited for the UV observation of BrO because of the high sensitivity and their intrinsic relatively high temporal resolution. Cox et al. [22] scanned the spectrum employing a photomultiplier. Wahner et al. [20], Orlando et al. [23], and Gilles et al. [24] recorded the UV absorption spectrum using a grating spectrograph with a diode array detector.

However, the wavelength deviations of grating spectrometers in the UV quite often lead to errors during the analysis of atmospheric observations. In an inter-comparison of several retrieval methods for remote sensing data, Aliwell [27] concluded that one of the major sources of error is the spectral calibration of the BrO reference data. Some studies have chosen high-resolution methods to record UV absorption spectra of BrO. Wheeler et al. [28] employed the sensitive cavity-ring-down spectroscopy technique, while Wilmouth et al. [29] used a continuous-scan interferometer for recording high-resolution FT-UV spectra. However, both these studies did not determine the absolute absorption cross-sections, but relative absorption spectra. Wilmouth et al. [29] scaled their spectra using literature values, made at a different spectral resolution. Wheeler and Wilmouth further carried out an elaborate rotational analysis and determined rotational constants and pre-dissociation lifetimes for the electronic state $A^2\Pi_{3/2}$. Wilmouth also estimated the upper and lower state dissociation energies. Nevertheless, no vibrational constants for the $A^2\Pi_{3/2}$ state have been reported so far from FTS measurements. These constants were determined in earlier works by Durie and Ramsay [46] and Barnett et al. [49] using grating spectrographs.

Thus far, few measurements of the UV absorption cross-section of BrO have been reported for stratospheric temperatures. The first low temperature absorption spectrum was recorded by Wahner et al. [20] at 223 K. This spectrum has been used in the past for atmospheric remote-sensing of BrO (after wavelength shifting by up to 0.2 nm). The only available spectra that cover a broader stratospheric temperature range from 203 to 273 K were recorded by Gilles et al. [24] employing a grating spectrograph.

In the present paper, the results from a flash photolysis study are reported. The recently developed technique of time-windowing Fourier transform spectroscopy (TW-FTS) [33] has been used to record UV absorption spectra of BrO at temperatures of 203, 223, 243, 273, and 298 K. The UV absorption cross-section of BrO was determined from a knowledge of the experimental absorption and the concentration of BrO as a function of time, the latter being determined by a chemical kinetics model. Moreover, the vibrational constants ω_e, x_e, and y_e, as well as the dissociation limit for the electronic state $A^2\Pi_{3/2}$ were analyzed.

2. Experimental

BrO was produced by a flash photolysis of mixtures of Br_2 and O_3. A schematic diagram of the apparatus is provided in Fig. 1. The photolysis setup had already been used for several studies [31,32]. For the experiments described here, it was synchronized to a continuous-scan FTS which is sketched in the lower part of Fig. 1. The Br_2 photosensitized decomposition of ozone was initiated in a quartz vessel of 3 l volume and 120 cm length by a broadband flash. The reaction vessel comprised three quartz tubes, the inner reaction volume being surrounded by two concentric jackets. The reaction volume was maintained at temperatures between 203 and 298 K by flowing ethanol or water through the inner jacket. The flow and temperature of the ethanol was controlled by a cryogenic cooler (Haake KT90-4). The outer jacket was evacuated to isolate thermally the inner compartments. All experiments were performed under flow conditions. The resultant flushing of the mixture minimized any secondary reactions and maintained the concentrations of the reactant gases, which are partially exhausted by radical reactions initiated by the photolysis flash. The gas inlet and the pump connection were located at the opposite ends of the reaction vessel.

The precursor mixtures of Br_2 and O_3 were transported through Teflon tubes. N_2 was used as carrier gas for Br_2. A part of the N_2 stream passed a cooled trap containing pure Br_2. The desired precursor concentrations were regulated by changing the carrier gas flow using flow controllers (MKS 1259 CC). The N_2 flow was between 100 and 1000 standard cm^3/min^{-1}. For the generation of O_3, a flow of O_2 passed through an electric discharge tube. The O_2 flow was regulated to between 100 and 4000 standard $cm^3\,min^{-1}$. The enrichment with O_3 in the discharge was between 0.5 and 3%, depending on the throughput of O_2. A second N_2 flow of between 500 and 6000 standard $cm^3\,min^{-1}$ was added in order to maintain the total pressure of 100 mbar. The purity of the gas sources was 99.998% for O_3 and 99.999%

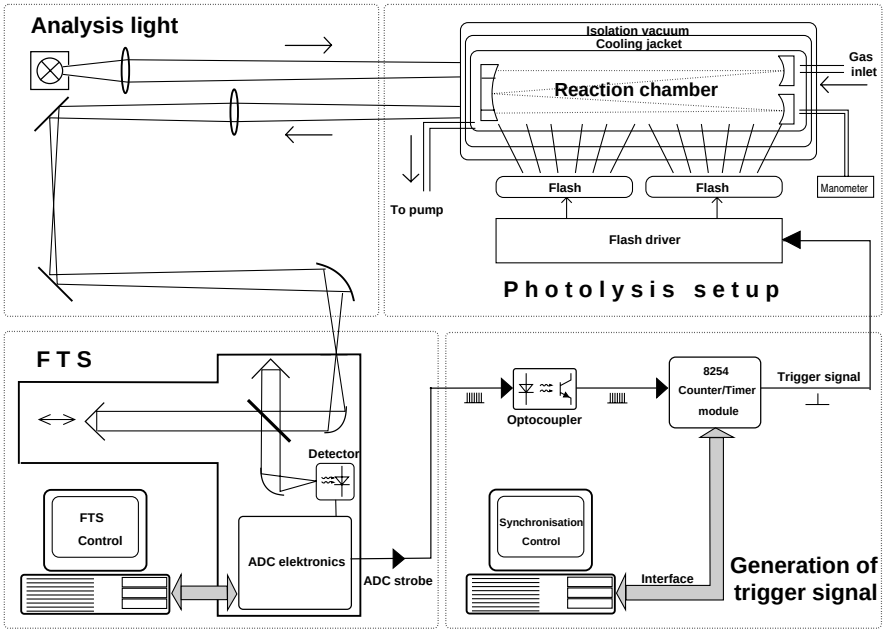

Fig. 1. Experimental setup. The upper part of the diagram shows the photolysis apparatus and the optical system for the absorption measurements. In the lower half, a continuous-scan FTS and the synchronization electronics are drawn. The synchronized trigger is used to start the photolysis flash.

for N_2 (Messer Griesheim, Germany). The precursors were mixed at a junction 0.5 m before entering the reaction vessel, which corresponded to a travel time of 3–10 ms. The total pressure in the cell was measured by a manometer (MKS Baratron 122 B, 1000 mbar, readout PDR-C-2C), connected directly to the absorption cell. After leaving the reaction chamber, the exhaust gases passed over a hot platinum wire to destroy the O_3 and other hazardous material. A cooled trap before the pump captured the residue of Br_2 and BrO. Chemical kinetics simulations were carried out prior to the experiments in order to estimate the required precursor concentrations. The concentrations were chosen such that the time constant for the formation of BrO was in the range 1–10 ms. This enabled the time-resolved observation with a temporal resolution of 0.333 ms. Initial concentrations of the precursors ranged from 1.0×10^{14}–5.4×10^{15} molecules/cm^3 for Br_2 and 1.0×10^{14}–1.8×10^{15} molecules/cm^3 for O_3. The maximum concentration of BrO was between 5.0×10^{12}–1.0×10^{14} molecules/cm^3, which corresponded to optical densities between 0.05 and 1.0.

Reactions were started by a broadband xenon photolysis flash. This flash was generated by a system comprising two flash tubes (Heimann HG-9903), positioned along the absorption cell, and the necessary electronics. The flash lamps were triggered by the synchronization signal from the TW-FTS control unit. The broadband emission of the flash tubes from 250 to 700 nm led to photodissociation mainly of Br_2. The photolyzed fraction of Br_2 was $0.80 \pm 0.11\%$ per flash. It was determined by comparing spectra from time windows directly before and after the flash. The photolyzed percentage turned out to be independent from the temperature within the stated error interval. To suppress the photolysis of O_3 resulting from absorption in the Hartley and Huggins bands, an appropriate plastic film was used as UV filter. The transmission spectrum of the plastic film decreased sharply at wavelengths below 320 nm, its optical density (OD) rising from 0.2 at 340 nm to more than 4.0 at 280 nm. However, the photolysis of some O_3 cannot be completely avoided, since O_3 also absorbs by its Chappuis band (400–800 nm) which lies in the same spectral region as the Br_2 absorption. In the experiments described here, the photolyzed fraction of O_3 was $0.051 \pm 0.020\%$. The photolysis flash had a duration of about 80 ± 30 μs (full width at half maximum), limited by impedances in the discharge electronics and by the condensers. Until 0.5–0.7 ms after the trigger, electrical cross-talk and scattered light from the flash disturbed the measurement. Therefore, the first two time windows could not be properly exploited. Since the typical time constants of the BrO formation were adjusted to 1–10 ms, the production of BrO, its maximum and subsequent removal could be readily observed with TW-FTS. The chain reactions initiated by the flash led to a catalytic destruction of a part of the O_3. In order to refill and re-establish the initial gas concentrations in the flow cell, a delay of 7.5 s was inserted before re-triggering the flash.

The absorption behavior after photolysis of the Br_2/O_3 mixtures was observed by time-resolved FTS measurements in the UV and visible spectral range. A high-pressure xenon lamp (Hamamatsu L2194, 75 W) was used as analysis light source, which is much weaker than the flash lamps. The reaction cell was equipped with an internal multi-path White-type optics comprising aluminium mirrors coated with MgF_2. The mirrors were mounted internally in order to reduce signal losses by the cell windows.

However, the mirror reflectivity of about 90% imposed a limitation on the absorption path length, set to 965.0 and 482.5 cm.

2.1. Time-windowing Fourier transform spectroscopy

The absorption measurements were carried out using a recently developed technique of time-windowing Fourier transform spectroscopy. This method is described in more detail elsewhere [33], therefore only a short summary is given here. The displacement of the sweep mirror of a continuous-scan FTS is monitored and a trigger signal is produced when the mirror reaches a certain position (Fig. 1). The TW-FTS technique has been implemented on a commercial Bruker IFS-120 HR Michelson interferometer. In the experiments described here, the trigger is employed to initiate the xenon flash of the photolysis setup. In this way, the chemical reactions are synchronized to the data acquisition of the FTS. The experiment has to be repeated while the trigger position with respect to the start of the interferogram is successively altered.

Eventually, the TW-FTS experiments yielded a series of interferograms which included the information for all time windows. From the raw-data, intensity spectra were derived as a function of time. Optical densities were then calculated for several time windows after the flash. As reference background for the optical densities, a time window spectrum recorded immediately before the trigger was used. This time window represented the undisturbed filled gas compartment about 5 ms before triggering the flash. Thus, the optical density spectra reflected the relative changes as a result of the photolysis flash and subsequent reactions. They were negative or positive when an absorber was removed, as for example O_3, or produced, like BrO. To obtain absolute optical density spectra, one absorption spectrum for a time window before the flash was compared to the spectrum of an empty cell. The resultant spectrum was added to the time-resolved optical densities. Since the FTS was evacuated during the measurements, all recorded spectra are calibrated in vacuum wavenumbers. The total spectral range extended from 16 000 cm^{-1} (625.0 nm) to 35 000 cm^{-1} (285.7 nm). The low wavenumber side of the spectrum was limited by the GaP detector diode, whereas the high wavenumber side was limited by the output of the analysis lamp.

Fig. 2 illustrates the temporal behavior of the optical density spectra and the formation and decay of different substances. Stray light from the photolysis flash can be observed in the spectrum at the experimental time around 0 ms. The flash is followed by the formation of BrO, which can be identified by the structured absorption between 25 000 and 33 000 cm^{-1}. The Br-catalyzed removal of the UV absorber O_3 is observed in the Huggins absorption bands between 31 000 and 36 000 cm^{-1}. The Br_2 absorption remains almost constant, since less than 1% is photolyzed. Three absorbers are clearly identified in the spectral region investigated: the precursors O_3 and Br_2 and the absorption bands of BrO.

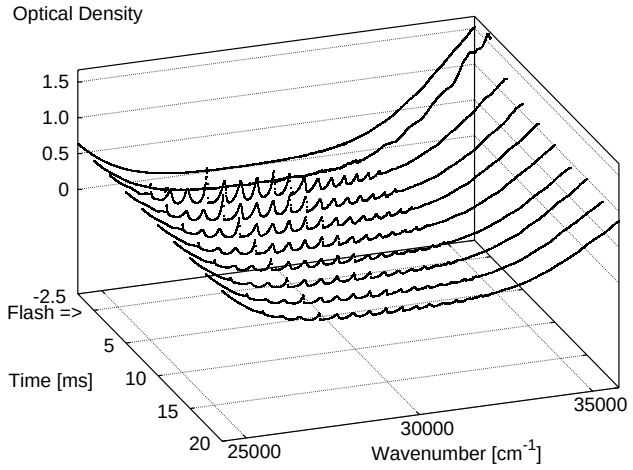

Fig. 2. Temporal series of optical densities recorded after applying a photolysis flash to a Br_2/O_3 mixture. The flash is triggered at time 0 ms. One spectrum for every 2.5 ms is plotted.

Two different series of flash photolysis experiments with time-resolved observation were carried out. The objective of the first series of measurements was to derive the UV absorption cross-section of BrO. The temporal resolution was set to 0.333 ms. In order to limit the total measurement time and the amount of experimental data, the spectral resolution was set to 40 cm^{-1}. This spectral resolution is sufficient to identify and resolve the vibrational bands in the $A^2\Pi_{3/2} \leftarrow X^2\Pi_{3/2}$ electronic transition of BrO. Experimental concentration decay curves of O_3 and Br_2 were determined from the respective changes in optical density. The required absorption cross-sections for O_3 were taken from Ref. [34], whereas the absorption spectra for Br_2 were determined from FTS measurements which were subsequently scaled to the absorption cross-sections reported in Ref. [35]. In these experiments, the kinetic parameters needed to infer the concentration, e.g. the photolysis rate of Br_2 and the loss of BrO were determined. This enabled the relative absorption spectrum to be transformed into absolute UV absorption cross-sections.

In a second series of TW-FTS measurements, UV absorption spectra of BrO were recorded with a spectral resolution of 3.8 cm^{-1} which is adequate for remote sensing applications. Again there was a trade-off between spectral and temporal resolution. The width of a time window was now set to 2.66 ms. Optical densities were accumulated and contributions of O_3 and Br_2 were removed. This yielded absorption spectra of BrO with a signal-to-noise ratio between 50 and 150. Using the results from the kinetic experiments described above, the optical densities were scaled to yield the absolute absorption cross-sections of BrO.

2.2. Determination of σ_{BrO}

In order to scale the relative spectra to absolute absorption cross-sections, the photolysis experiments had to be

interpreted by a chemical kinetics model. The chemical mechanism, used in the data analysis, comprises the homogeneous gas-phase reactions that dominate the reaction system of Br_2, O_3, and BrO. They have been reported by several authors [25,26,36,37]. BrO was formed through the bromine-photosensitized destruction of ozone:

$$Br_2 + h\nu \rightarrow 2Br \quad (1)$$

$$Br + O_3 \rightarrow BrO + O_2 \quad (2)$$

The photolysis of Br_2, reaction (1), was not modeled explicitly. Instead, the initial amount of Br atoms was determined from the fraction of photolyzed Br_2 ($0.80 \pm 0.11\%$ per flash). BrO was formed mainly by reaction (2). However, since the photolysis of O_3 could not be suppressed completely, a small amount of BrO was also formed by the reaction of $O(^3P)$ atoms with Br_2:

$$O_3 + h\nu \rightarrow O(^3P) + O_2 \quad (3)$$

$$O(^3P) + Br_2 \rightarrow BrO + Br \quad (4)$$

Reaction (4) is again followed by reaction (2), forming another BrO molecule in the presence of ozone. The photolyzed fraction of O_3 was determined to $0.051 \pm 0.020\%$ per flash. Because photolysis wavelengths shorter than 320 nm were filtered by a plastic film, atomic oxygen was expected to be formed mainly as $O(^3P)$. The remaining $O(^1D)$ atoms were supposed to be quenched to $O(^3P)$.

Three different approaches were used to scale the relative spectra of BrO to absolute absorption cross-sections σ_{BrO}. The first method was based on a budget consideration. In a first approximation, the amount of BrO produced by the flash can be regarded as being given by the quantity of photolyzed precursor molecules. Considering the concentration of Br and O atoms immediately after the flash, and the BrO forming reactions (2) and (4), the expected concentration of BrO was estimated through $[BrO] = [Br] + 2[O]$. The absorption cross-section of BrO could then be calculated by $\sigma_{BrO} = OD/[BrO]L$, where L is the absorption path length and the optical density.

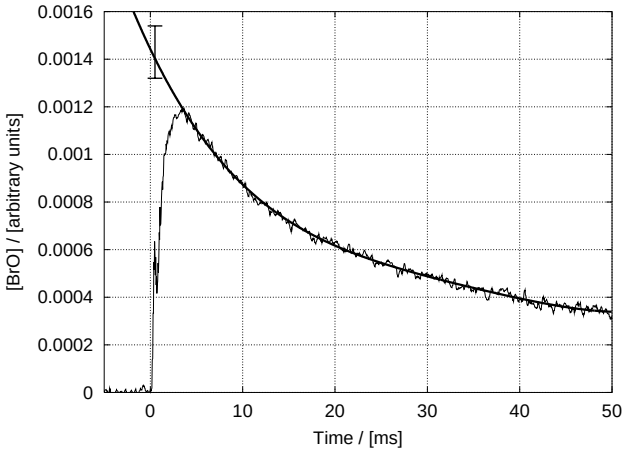

Fig. 3. Decay curve of the relative BrO concentration. For a comparison of the BrO concentration with the precursor budget, the decay curve has been back-extrapolated to 0.2 ms.

The production of BrO after the photolysis flash was not instantaneous, but was characterized by a rising slope. Simultaneously with the formation of BrO, the self-reactions (see reactions (5) and (6) below) led to a partial disintegration of BrO. This mechanism caused a maximum observed concentration of BrO at about 3–10 ms after the flash trigger. Beyond that maximum, the BrO concentration slowly decayed (Fig. 3). For the budget calculation, the virtual optical density of BrO immediately after the flash had to be determined. This was done by extrapolating the decay curve of BrO back to the moment right after the flash at about 0.2 ms. An example for this backwards extrapolation is shown in Fig. 3. The concentration is given in relative units, because at this state of the analysis, no absolute concentration measurement was possible. Using a polynomial of fourth grade, the decay curve was back-extrapolated to 0 ms, the time of the flash trigger.

The results for the peak absorption cross-section in the (7, 0) band of BrO ($29\,540\,cm^{-1}$) are given in Table 1 (row 1) for a spectral resolution of $3.8\,cm^{-1}$. The results from other methods of data analysis that are discussed in

Table 1
Experimental results for the UV absorption cross-sections of BrO, derived by different methods from the TW-FTS measurements

	Temperature (K)				
	203 ± 3 (12)	223 ± 3 (14)	243 ± 3 (16)	273 ± 2 (17)	298 ± 2 (26)
Precursor budget	2.50 ± 0.78	2.14 ± 0.70	2.25 ± 0.54	2.02 ± 0.38	2.00 ± 0.68
Second-order decay[a]	4.5 ± 2.8	3.9 ± 2.7	3.4 ± 1.6	2.8 ± 1.5	1.8 ± 0.9
Second-order decay[b]	4.1 ± 1.8	3.5 ± 1.4	3.7 ± 1.1	2.4 ± 0.9	1.5 ± 0.9
Chemical kinetics simulation[c]	3.31 ± 0.83	2.74 ± 0.69	2.39 ± 0.47	2.18 ± 0.46	2.17 ± 0.51
Chemical kinetics simulation[d]	3.03 ± 0.31	2.75 ± 0.29	2.52 ± 0.26	2.23 ± 0.23	2.19 ± 0.23

The results are given for the peak absorption of BrO in the (7, 0) vibrational band at $29\,540\,cm^{-1}$ (338.5 nm) and a spectral resolution of $3.8\,cm^{-1}$ FWHM. The units are $10^{-17}\,cm^2$ per molecule. The error intervals represent two times the standard deviation. Values in parentheses are number of experiments.

[a] The values were calculated using k_6 as reported in Ref. [41] (see Table 2).

[b] The values were calculated based on the TW-FTS results for k_6.

[c] Measurements were averaged for each temperature separately.

[d] The integrated absorption cross-sections of all temperatures were averaged (see text).

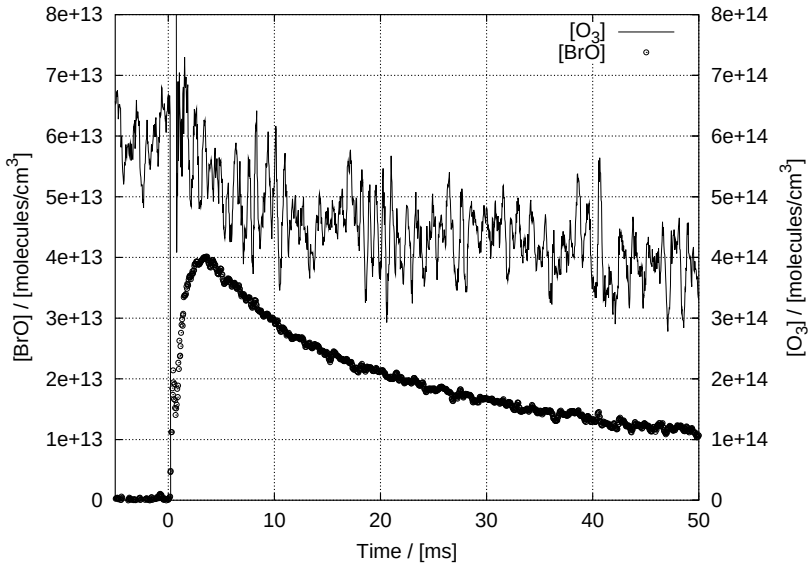

Fig. 4. Concentration–time profiles of BrO and O_3, recorded in a TW-FTS measurement at 273 K.

the following sections are also stated. For 203 and 223 K, the cross-sections from the precursor budget are lower than the values reported by previous studies, whereas for high temperatures the results are comparable (Table 5, Refs. [20,22–24,26,29]). At 298 K, the peak cross-section of the (7, 0) band yields $(1.39 \pm 0.48) \times 10^{-17}$ cm^2 per molecule at a spectral resolution of 36 cm^{-1} (0.40 nm) and a confidence interval of 2σ. This is only 12% smaller than the average value from the mentioned studies, 1.58×10^{-17} cm^2 per molecule. On the other hand, at 223 K, the back-extrapolation yields $(1.35 \pm 0.44) \times 10^{-17}$ cm^2 per molecule at a spectral resolution of 36 cm^{-1}, which is 30% smaller than the value reported by Wahner et al. [20], and about 40% below the result from Gilles et al. [24].

In a second analysis of the experimental data, the decay curve of the BrO concentration was investigated. The decrease of BrO is caused by the self-reactions:

$$\mathrm{BrO} + \mathrm{BrO} \rightarrow 2\mathrm{Br} + \mathrm{O_2} \quad (5)$$

$$\mathrm{BrO} + \mathrm{BrO} \rightarrow \mathrm{Br_2} + \mathrm{O_2} \quad (6)$$

In a study of the BrO self-reaction, Harwood et al. [38] observed an additional absorber with an unstructured spectrum at the temperatures 223 and 235 K and pressures above 133 mbar. It was attributed to the BrO-dimer Br_2O_2. Harwood et al. also observed a pressure dependence of the self-reaction in the pressure range from 133 to 1013 mbar, and therefore proposed a third channel of the self-reaction, $2\mathrm{BrO} + \mathrm{M} \leftrightarrow \mathrm{Br_2O_2} + \mathrm{M}$. However, the TW-FTS experiments showed no evidence for an additional absorber. Only three absorbers could be distinguished above noise level. They were identified as Br_2, O_3, and BrO. A reason for this is supposedly the lower pressure of 100 mbar. As discussed below, this was also supported by a plot of 1/[BrO] against time (Fig. 5).

In Fig. 4, the experimental concentration–time profiles of BrO and O_3 are plotted for a measurement at 273 K. The O_3 concentration decays slowly due to the catalytic destruction cycle formed by reactions (2) and (5). The initial concentration of O_3 was 1.0×10^{14}–1.8×10^{15} molecules/cm^3 and thus between 10 and 100 times bigger than the amount of Br atoms. As observed in several previous studies [22,25,30,36,38], an excess concentration of ozone leads to a masking of reaction (5), because almost every produced Br atom reacts with O_3 via reaction (2) to form another BrO. Hence, the observable decay of BrO is supposedly caused by reaction (6) only. The concentration curve of BrO may then be expressed as a second-order decay because of the self-reaction (6):

$$\frac{1}{[\mathrm{BrO}]_t} = \frac{1}{[\mathrm{BrO}]_0} + 2k_6 t \quad (7)$$

Fig. 5 shows the optical density and the corresponding concentration of BrO, plotted as 1/OD and 1/[BrO] against time for a measurement at 223 K. The graph is almost straight and supports the model of a simple second-order decay. The small structures in the plot are caused by some instability during the TW-FTS measurement. Similar plots with little or no curvature were obtained for the other temperatures. As pointed out by Harwood et al. [38], this indicates that ter-molecular reactions were not observable, and presumably no large quantities of Br_2O_2 were formed. The appearance of Br_2O_2 should instead lead to a convex curve.

The experimental concentration [BrO] and the absorption cross-section σ_{BrO} are related through $\mathrm{OD} = [\mathrm{BrO}]\sigma_{\mathrm{BrO}}L$, where OD is the measured optical density and L the absorption path length. The slope of Fig. 5 can be used to determine the relation $k_6/\sigma = L\Delta(1/\mathrm{OD})/(2\Delta t)$. Further, with knowledge of k_6, the UV absorption cross-section of BrO can be derived. Values for k_6 were taken from DeMore

et al. [41], and the absorption cross-section of BrO was scaled accordingly. The example of Fig. 5 yields $\sigma_{BrO} = 3.14 \times 10^{-17}$ cm^2 per molecule for the peak absorption in the (7, 0) vibrational band at 29 540 cm^{-1} and a spectral resolution of 3.8 cm^{-1} (FWHM). The results for all temperatures are stated in the row 2 of Table 1. All experiments of one temperature were averaged. A second data analysis to determine σ_{BrO} was carried out using the TW-FTS results for k_6 from the chemical kinetics simulation as described in the next section. The values are stated in row 3 of Table 1. The error intervals for σ_{BrO} reflect the uncertainty of k_6 and the experimental errors in the determination of the slope of the function 1/OD versus time. The average values for k_6 as stated in Table 2 have been reported by DeMore et al. [41]. The error ranges of k_6 were chosen after a comparison of different studies of the self-reaction of BrO by Cox et al. [22], Mauldin et al. [30], and Harwood et al. [38]. However, the accuracy of the absorption cross-section of BrO as determined by the decay analysis is not satisfying. The error intervals for σ_{BrO} are between ±30 and ±60%, based on a 95% confidence level.

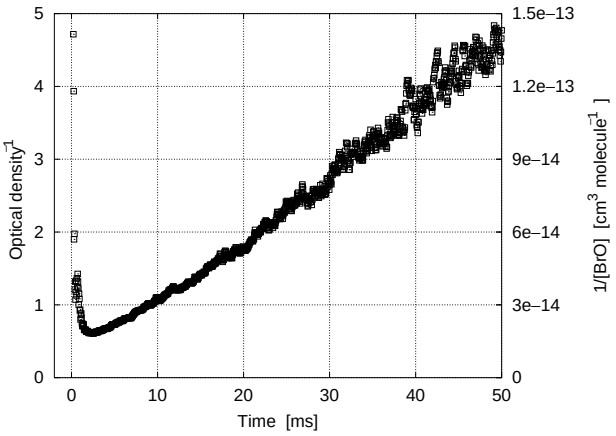

Fig. 5. Experimental decay curves of the optical density and the concentration of BrO for a measurement at 223 K. The data are plotted as 1/[OD] at 29 540 cm^{-1} and 1/[BrO] against time.

The large inaccuracy of the decay method made it necessary to extend the chemical model and perform a chemical kinetics simulation of the experiments. The experimental concentration–time profiles of BrO and O_3 were compared to the modeled decay curves. For the simulation, additional reactions were included. Br_2 is produced mainly by the self-reaction of BrO (6). Another mechanism of Br_2 formation was proposed by Laszlo et al. [26], who assumed a production of Br_2 which is catalyzed by BrO:

$$Br + BrO \rightarrow Br_2O \quad (8)$$

$$Br + Br_2O \rightarrow Br_2 + BrO \quad (9)$$

Laszlo et al. [26] determined k_8 to be $(1.5 \pm 0.4) \times 10^{-12}$ cm^3 per molecule s at room temperature. The rate of reaction (9) was measured by Burkholder [39] to $k_9 = 2 \times 10^{-10}$ cm^3 per molecule s. Reaction (8) is considerably slower than reaction (9) and therefore limits the rate of the Br_2 formation. Since a small part of the ozone was also photolyzed, reactions involving atomic oxygen were included in the model:

$$O(^3P) + BrO \rightarrow Br + O_2 \quad (10)$$

$$O(^3P) + O_2 + M \rightarrow O_3 + M \quad (11)$$

$$O(^3P) + O_3 \rightarrow O_2 + O_2 \quad (12)$$

Reaction (10) can remove BrO and form Br, which in turn can react with the remaining O_3 via reaction (2). In this way, BrO is recycled and another O_3 molecule decomposed. Reaction (11) produces O_3, and through reaction (12), odd oxygen is removed.

The chemical kinetics model was simulated using the integrator of differential equations facsimile [40]. Rate constants

Table 2
Experimental results and literature values for the rate constants k_5 ($\times 10^{-12}$ cm^3/s molecule) and k_6 ($\times 10^{-13}$ cm^3/s molecule)

	Temperature (K)				
	203 ± 3	223 ± 3	243 ± 3	273 ± 2	298 ± 2
k_5					
This work	2.1 ± 1.2	2.9 ± 0.8	2.7 ± 1.0	3.0 ± 0.8	2.9 ± 0.6
[41]	2.92	2.87	2.83	2.78	2.74
[38]				2.45 ± 0.54	2.62 ± 0.57
[30]		1.23			2.34 ± 0.43
[22]				3.0 ± 2.4	3.4 ± 2.6
[37]					2.49 ± 0.42
k_6					
This work	16.8 ± 4.0	11.9 ± 2.8	10.6 ± 1.6	5.6 ± 1.2	4.1 ± 2.4
[41]	19.4	13.2	9.6	6.5	5.0
[38]		8.3	6.4	4.3	3.1
[30]		5.8			4.45 ± 0.82
[22]				7.4 ± 1.6	6.6 ± 2.0
[37]					4.69 ± 0.68

The TW-FTS results are stated in the top lines.

were taken from the Refs. [22,26,30,38,41]. Other input parameters were the initial concentrations of Br, O(^{3}P), Br_2, and O_3 after the photolysis flash. The output of the chemical model was compared to the experimental concentration time profiles of BrO and O_3. Based on the least squares differences and a genetic fitting algorithm, the model parameters were optimized. The employed fitting algorithm is capable of finding the global optimum in a given parameter space, being rather independent of initial parameter settings. Three fit-parameters were optimized simultaneously: the scaling factor for the BrO absorption cross-section and the rate constants of the self reactions (5) and (6). The rate constants k_5 and k_6 were determined because the confidence intervals stated in the literature [22,30,38,41] allow a large variation of between ±20 and ±50% (see Table 2). Moreover, a sensitivity analysis which is described below, indicated that the absorption cross-section of BrO depends to a large extent from the rates of the reactions (5) and (6) (compare Table 4). The same is true for reaction (2), which is responsible for the initial formation of BrO directly after the photolysis flash. However, the first two time windows up to 0.7 ms were disturbed by stray light and electrical cross-talk from the flash driver and cables. This made the observation of the rising slope of the BrO concentration difficult. Therefore, the rate constant k_2 as reported in Ref. [41] was used ($k_2 = 1.7 \times 10^{-11} \exp(-800/T)$ cm^3/s molecule).

The experimental results for the rate constants k_5 and k_6 are listed in Table 2. As a comparison, the values reported in the Refs. [22,30,37,38,41] are also stated. The ter-molecular channel of the self-reaction of BrO as proposed by Harwood et al. [38], $2BrO + M \leftrightarrow Br_2O_2 + M$, was included in the chemical model. For this reason and because of the lower pressure (100 mbar), we expect that the TW-FTS results for k_5 and k_6 do not have contributions from the third channel.

For room temperature, the experimental results are in agreement with the literature values. As mentioned before, the high experimental concentration of ozone led to a masking of reaction (5). Although this reaction was almost invisible, Table 2 shows that the results for k_5 are comparable to most of the other studies. For k_6 at temperatures below 250 K, the values reported by Harwood et al. [38] and Mauldin et al. [30] are smaller than the TW-FTS results. The could not be totally explained by our measurements. The low temperature results by Mauldin et al. [30] for both k_5 and k_6 are also not in agreement with other studies. In the Figs. 6 and 7, the TW-FTS results for k_5 and k_6 are plotted in the Arrhenius form as ln(k) over 1/T. The average values from DeMore et al. [41] are drawn as well. With exemption of the measurements at 203 K, the figures indicate a good agreement between the TW-FTS results and the literature values.

The temperature dependence of a rate constant k can be expressed as $k = A \exp(-E_a/RT)$ with the Arrhenius parameter A and the activation temperature $T_a = E_a/R$. The Arrhenius parameters for k_5 and k_6 were derived from a linear regression. The results are summarized in Table 3. Within the error intervals, the TW-FTS results for k_6 are in agreement with the values reported by DeMore et al. [41] and Harwood et al. [38]. For k_5, the broad error interval of the activation temperature E_a/R is caused by the measurement at 203 K (Fig. 6). Apart from that, the literature values for both k_5 and k_6 show a large variation. Few measurements have been reported for lower temperatures. Mauldin et al. [30] investigated room temperature and only one lower temperature (223 K). Cox et al. [22] carried out measurements at elevated temperatures (273–348 K). And since the pre-exponential factor A generally is not independent of the temperature over a broader range, the results by Cox are not quite comparable to the other studies.

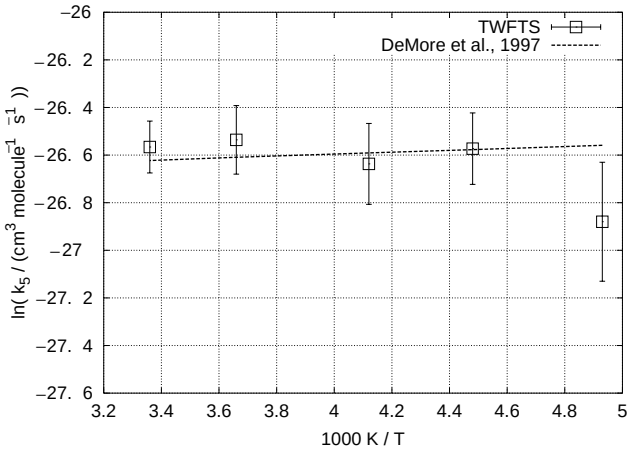

Fig. 6. Experimental results for k_5, plotted as ln k_5 vs. 1/T. The straight line indicates the values reported by DeMore et al. [41].

The third parameter from the optimization yielded the scaling factors for the BrO absorption cross-sections. Using the results from the chemical kinetics simulation, the high-resolution optical density spectra were transformed to cross-sections. All measurements of one temperature

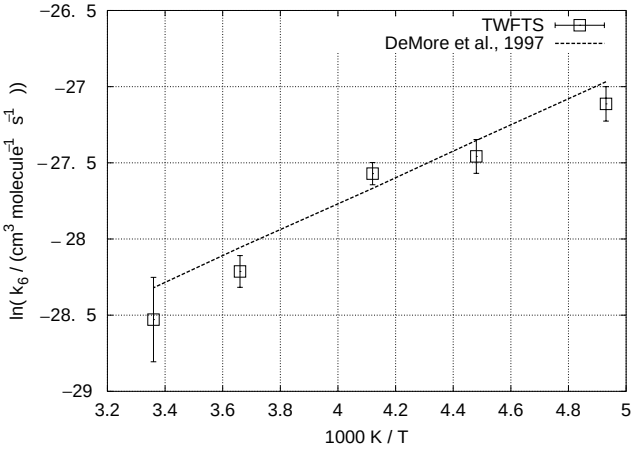

Fig. 7. Experimental results for k_6, plotted as ln k_6 vs. 1/T. The straight line indicates the values reported by DeMore et al. [41].

Table 3
Arrhenius parameters for the rate constants k_5 and k_6

Constant	Reference	A ($\times 10^{-13}$ cm^3/s molecule)	E_a/R (K)
k_5	This work	33.0 ± 7.9	36 ± 55
k_5	DeMore et al. [41]	24	40
k_5	Harwood et al. [38] (T > 250 K)	53.1 ± 11.7	−211 ± 59
k_5	Cox et al. [22]	120	375 ± 415
k_6	This work	0.210 ± 0.113	−905 ± 104
k_6	DeMore et al. [41]	0.28	−860
k_6	Harwood et al. [38] (T > 250 K)	0.113 ± 0.047	−983 ± 111
k_6	Cox et al. [22]	2.9	−259 ± 208
k_6	Mauldin et al. [30] (135 mbar)	2.01	−237

The TW-FTS error intervals represent the standard deviation from the linear regression.

were averaged. The results are stated in row 4 of Table 1 for the peak cross-section of the (7, 0) band at a spectral resolution of 3.8 cm^{-1}. In the top line, the number of measurements for each temperature is given. The error intervals of σ_{BrO} are caused by two factors. The first contribution is the averaging of several measurements. The second part results from the uncertainty of the parameters used in the chemical kinetics simulation. In order to determine the effect of these uncertainties in the data evaluation on the UV absorption cross-section of BrO, a sensitivity analysis was carried out. The mathematical weight of the photolysis and the reactions in the chemical kinetics model was investigated. Experimental uncertainties resulted from the photolyzed fractions of the precursors Br_2 (0.80 ± 0.11% per flash) and O_3 (0.051 ± 0.020%). Inaccuracies of the chemical kinetics model originate from the employed rate constants. The sensitivity analysis was carried out by changing one parameter at a time within its allowed interval. A new fit of the chemical kinetics model to the experimental data then yielded a changed value for the UV absorption cross-section of BrO. The results of the sensitivity analysis are listed in Table 4, expressed as relative changes in the absorption cross-section due to the variation of one parameter.

The uncertainty in the amount of Br atoms produced by the photolysis of Br_2 was a major experimental source of error. The absorption cross-section of BrO varied by 6–9%, depending on the amount of photolyzed Br_2. On the other hand, the imprecise determination of the O_3 photolysis contributed by between 0.3 and 1.3% to the error in σ_{BrO}. Table 4 further indicates that reactions (2), (5), and (6) which dominate the kinetics of the BrO radical in the regarded temperature range have the biggest impact. The inaccuracy of the rate of self-reaction (6) has most influence at lower temperatures. Contrarily, reactions (4), (10), (11), and (12), which involve atomic oxygen, only have a small effect on the absorption cross-section. The error contributions of all parameters listed in Table 4 sum up to the total uncertainty which is stated in the bottom line. The resulting error in the determination of σ_{BrO} from one measurement is between 13 and 22% on a confidence level of 95%. The total error of σ_{BrO} for one temperature as stated in Table 1 (row 4) is between 20 and 26%. It includes the averaging of several measurements and the uncertainties of parameters.

3. Results and discussion

The absolute UV absorption cross-sections of BrO were determined by combining the relative spectra and the results from the chemical kinetics simulation. Fig. 8 shows most of the band system for the temperatures 203 and 273 K. It illustrates the population change of the rotational terms in the electronic ground state $X^2\Pi_{3/2}$ with varying temperature. For the lowest observed temperature, 203 K, the vibrational bands become very narrow, and the minimum absorption between the bands approaches zero. In particular, no underlying continuum is observable. The earlier study by Wahner et al. [20], suggested the existence of an absorption continuum below the observed band system. However, the new

Table 4
Relative changes of the UV absorption cross-section of BrO because of the uncertainty of parameters in the experiments or the data analysis

	T (K)				
	203 ± 3	223 ± 3	243 ± 3	273 ± 2	298 ± 2
$\delta\sigma_{k_2}$ (%)	10.3	10.0	7.9	7.6	10.4
$\delta\sigma_{k_4}$ (%)	0.16	0.14	0.11	0.19	0.19
$\delta\sigma_{k_5}$ (%)	4.0	3.4	3.2	4.7	5.6
$\delta\sigma_{k_6}$ (%)	16.6	13.6	11.2	6.3	5.4
$\delta\sigma_{k_8}$ (%)	2.8	2.6	2.0	1.8	4.5
$\delta\sigma_{k_9}$ (%)	0.25	0.34	0.14	0.32	0.18
$\delta\sigma_{k_{10}}$ (%)	0.03	0.14	0.09	0.04	0.04
$\delta\sigma_{k_{11}}$ (%)	0.16	0.14	0.23	0.07	0.06
$\delta\sigma_{k_{12}}$ (%)	0.13	0.01	0.14	0.04	0.17
$\delta\sigma_{Br_2}$ (%)	6.9	8.7	8.1	7.6	6.1
$\delta\sigma_{O_2}$ (%)	0.39	1.1	1.3	0.74	0.21
$\delta\sigma_{Par}$ (%)	21.4	19.6	16.5	13.5	15.0

The errors due to uncertainties of the rate constants are stated by $\delta\sigma_k$ (%). The effect of the photolysis of the precursors Br_2 and O_3 is given in the rows $\delta\sigma_{Br_2}$(%) and $\delta\sigma_{O_3}$ (%). Only one parameter was changed in each case. The bottom line lists the total uncertainty $\delta\sigma_{Par}$ (%) of one measurement including all parameter variations (95% confidence).

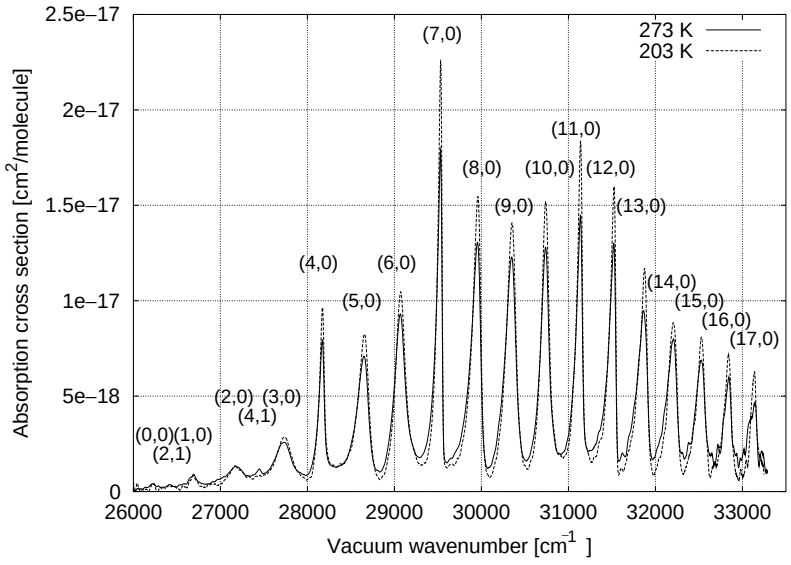

Fig. 8. Experimental UV absorption cross-section of BrO for the temperatures 203 and 273 K. The spectral resolution is 18 cm^{-1} (0.20 nm). The vibrational bands are labeled with the quantum numbers (v', v'') for the upper and lower states.

TW-FTS measurements as well as the results reported by Wilmouth et al. [29] provide no evidence for such a continuum. Both results indicate that the UV absorption spectrum is formed by the A–X band system only. Fig. 8 also shows the population change of the first excited vibrational state $v'' = 1$. The hot band (4, 1) at 27 470 cm^{-1} is considerably weaker at 203 K compared to 273 K.

When comparing the results for the different temperatures, we found that the integral of the UV absorption cross-section over the whole band system, $\int \sigma(\tilde{\nu})\, d\tilde{\nu}$, was approximately constant. The results of the integral are plotted in Fig. 11 for all investigated temperatures. The variation of the mean values is considerably smaller than the error bars for each temperature that represent twice the standard deviation. Supported by a spectroscopic reasoning which is discussed below, we expect that the integral varies by less than 1% within the temperature range from 203 to 298 K. Therefore, the results for all temperatures were averaged. The mean value of the integral is $(2.66 \pm 0.28) \times 10^{-14}$ cm per molecule, with a 2σ error interval. All absorption spectra were then scaled to this mean value. Taking into account the error intervals for every temperature, a standard deviation of 5.2% for the absorption cross-section was yielded. The results are stated in row 5 of Table 1 and in Table 5.

Table 5
A comparison of the experimental UV absorption cross-section of BrO from this work with other studies

Reference	Spectral resolution (nm)	Temperature (K)				
		203 ± 3	223 ± 3	243 ± 3	273 ± 2	298 ± 2
This work	0.042 nm / 3.8 cm^{-1}	3.03 ± 0.31	2.75 ± 0.29	2.52 ± 0.26	2.23 ± 0.23	2.19 ± 0.23
This work	0.20 nm / 18 cm^{-1}	2.33 ± 0.24	2.14 ± 0.22	2.01 ± 0.21	1.84 ± 0.19	1.82 ± 0.19
This work	0.40 nm / 36 cm^{-1}	1.86 ± 0.19	1.73 ± 0.18	1.64 ± 0.17	1.54 ± 0.16	1.52 ± 0.16
[22]	0.22 nm					1.8 ± 0.20
[20]	0.18 nm		2.21 ± 0.16			1.71 ± 0.14
[24]	0.50 nm	2.15	2.05	1.93	1.84	1.63
[26]	0.60 nm					1.41 ± 0.15
[25]	0.90 nm		1.56 ± 0.14			1.14 ± 0.14
[22]	0.40 nm					1.6 ± 0.18
[20]	0.40 nm		1.95 ± 0.15			1.55 ± 0.13
[23]	0.40 nm					1.4 ± 0.3
[24]	0.40 nm	2.30	2.21	2.06	1.96	1.74
[26]	0.40 nm					1.59 ± 0.18
[29]	0.40 nm		228 K: 1.97 ± 0.15			1.58 ± 0.12

The table lists the peak absorption cross-section of the (7, 0) vibrational band at 29 540 cm^{-1} (338.5 nm). Units are 10^{-17} cm^2 per molecule. The results are given for different spectral resolutions. The spectral resolution of the TW-FTS experiments was 3.8 cm^{-1} (0.042 nm at 330 nm). In the middle part of the table, results by different authors are listed at their original spectral resolution. For a better comparison, all values were transformed to a spectral resolution of 36 cm^{-1} or 0.40 nm (after [29]).

In most of the earlier studies on the UV absorption cross-section BrO, the results have been reported for the peak absorption of the (7, 0) vibrational band at 29 540 cm^{-1} (338.5 nm). Tables 1 and 5 therefore list the TW-FTS results for this peak. Table 5 compares the experimental results with previous studies. To obtain a comparable spectral resolution, the BrO spectra from the TW-FTS measurements were convoluted using a Gaussian function with an appropriate half-width. The results are presented for the original spectral resolution and for a common spectral resolution of 36 cm^{-1} (0.40 nm, FWHM). Note that the value reported by Wilmouth et al. [29] was calculated by averaging the results of the other studies listed in Table 5.

The new absorption cross-section of BrO at 298 K is in good agreement with the values reported by Cox et al. [22], Wahner et al. [20], Orlando et al. [23], and Laszlo et al. [26]. At deeper temperatures, the results of this study are generally below the values published by Gilles et al. [24], Wahner et al. [20], and Wilmouth et al. [29]. Further, the temperature dependence of the TW-FTS experiments is smaller than observed in the other measurements. Between 298 and 223 K, the values reported by Gilles for the (7, 0)-band peak cross-section increase by 27%. Within the same temperature range, the TW-FTS results rise by only 14% at 0.40 nm (36 cm^{-1}) spectral resolution. The temperature behavior for the peak cross-section was confirmed by a synthesis of the vibrational band (7, 0), as described below with the vibrational analysis. Although no absolute cross-sections could be determined from the synthesis, the temperature ratios were comparable to the TW-FTS results.

Fig. 9 shows the spectral region that is used for the determination of atmospheric concentrations of BrO from remote sensing data [9,42]. Again, the broadening of vibrational bands as well as the increase of the hot band (4, 1) with increasing temperature may be observed. In Fig. 10, the vibrational band (7, 0) is plotted for different stratospheric temperatures. It is one of the few bands in the band system of the A–X transition that show rotational structure. The rotational lines are broadened due to pre-dissociation. The linewidth was determined by Wheeler et al. [28] to 3.2 ± 0.3 cm^{-1} (FWHM).

3.1. Temperature dependence of the integrated cross-section

As noted above, when comparing the TW-FTS results for different temperatures, the integral $\int \sigma(\tilde{\nu})\,d\tilde{\nu}$ over the UV absorption cross-section of BrO was found to be almost constant. The integration was carried out in the range from 26 300 cm^{-1} (380.2 nm) to 35 000 cm^{-1} (285.7 nm). The experimental results for the different temperatures are plotted in the Fig. 11. Corresponding values for the studies by Wahner et al. [20] and Gilles et al. [24] are also included. While the integral values for the spectra by Wahner are comparable to the TW-FTS values, the results for Gilles are about 20% higher. Obviously, all experimental values show a rather small variation over the whole temperature range. The mean TW-FTS value over all five temperatures is $(2.66 \pm 0.28) \times 10^{-14}$ cm per molecule. The integral $\int \sigma(\tilde{\nu})\,d\tilde{\nu}$, when carried out over the entire band system of an electronic transition, is proportional to the Einstein coefficient for absorption and hence to the square of the dipole matrix element R^e for the electronic transition [43]:

$$\int \sigma(\tilde{\nu})\,d\tilde{\nu} = h\tilde{\nu}_{nm}\frac{8\pi^3}{(4\pi\varepsilon_0)3h^2}|R^e|^2 \quad (13)$$

Here, $\tilde{\nu}_{nm}$ is the mean wavenumber of the band system, h the Planck constant, and ε_0 the vacuum permittivity. According

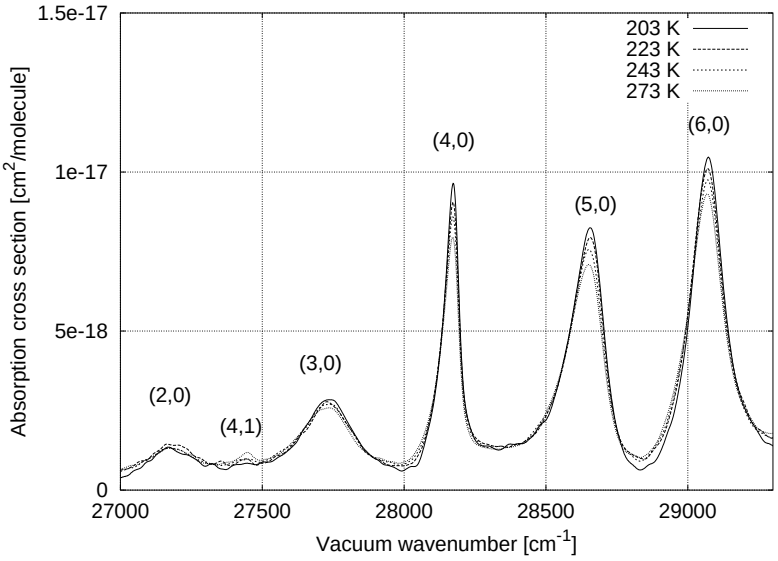

Fig. 9. UV absorption cross-section of BrO at stratospheric temperatures in the spectral region that is used for data retrieval in remote sensing. The spectral resolution is 18 cm^{-1} (0.20 nm). The vibrational bands are labeled with the quantum numbers (v', v'').

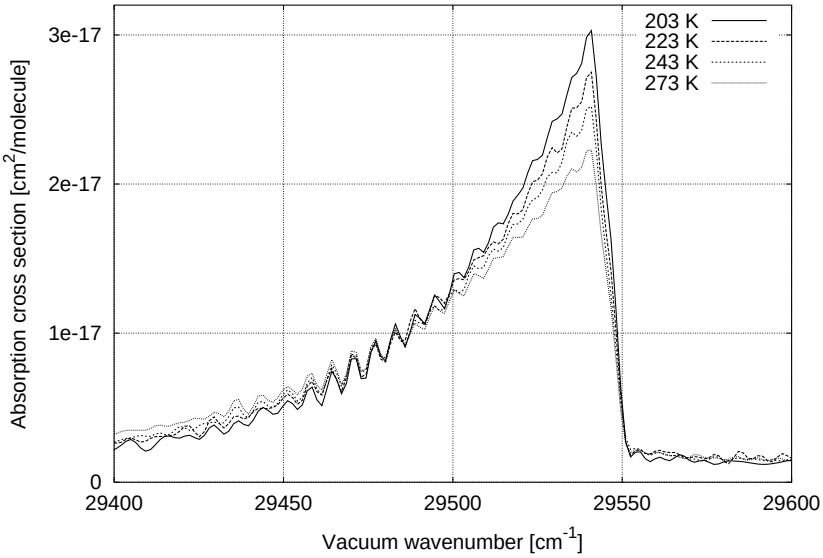

Fig. 10. UV absorption cross-section of BrO for the (7, 0) band at stratospheric temperatures. The spectral resolution is 3.8 cm^{-1} (0.042 nm).

to Born and Oppenheimer [44], Eq. (13) is independent of vibrational and rotational quantum numbers. Therefore, to understand the temperature behavior, only the electronic transitions have to be considered. This leads to two questions: (1) Which electronic transitions are involved in the observed UV absorption spectrum of BrO? (2) How big is the variation of R^e in the temperature range from 203 to 298 K? To answer the first question, the thermal distribution over several lower electronic states has to be discussed. For BrO, only the two electronic states, $X^2\Pi_{3/2}$ and $X^2\Pi_{1/2}$, are significantly populated at stratospheric temperatures. The doublet splitting was determined by McKellar [45] to 968 cm^{-1}. The energetically higher doublet term $X^2\Pi_{1/2}$ has a thermal population of 0.93% at 298 K and 0.10% at 203 K. For the UV spectrum of BrO, no absorption bands have been reported that could be assigned to the electronic transition $A^2\Pi_{1/2} \leftarrow X^2\Pi_{1/2}$. The observation of this sub-band is difficult because of the disturbing main transition $A^2\Pi_{3/2} \leftarrow X^2\Pi_{3/2}$, which is probably about 100 times stronger at 298 K due to the higher population. The two systems are expected to be located in the same spectral range. For ClO, both electronic transitions have been observed by Durie and Ramsay [46]. Hence, they can also be expected for BrO. However, caused by the small population, the sub-band $A^2\Pi_{1/2} \leftarrow X^2\Pi_{1/2}$ has very little impact on the integrated absorption cross-section at the con-

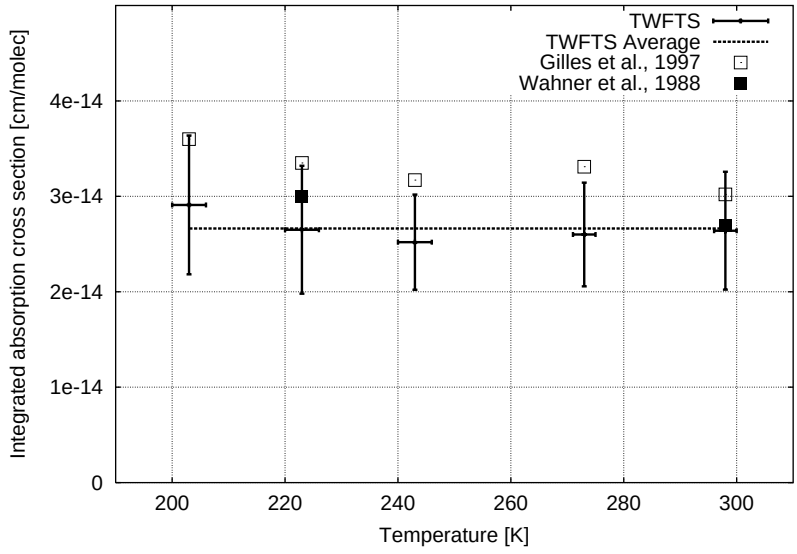

Fig. 11. Integrated UV absorption cross-section of BrO for different temperatures. The integration $\int \sigma(\tilde{\nu})\,d\tilde{\nu}$ extends from 26 300 to 35 000 cm^{-1}. The TW-FTS results are compared to the measurements by Wahner et al. [20] and Gilles et al. [24]. The horizontal line indicates the TW-FTS average over all temperatures. The error bars represent two times the standard deviation.

sidered temperatures. Since the transition dipole moments of the two sub-bands are probably similar, we estimate the variation to be much smaller than the population difference of 0.83%, when changing temperature from 298 to 203 K.

Eq. (13) further depends on the purely electronic matrix element R^e, which is related to the electronic eigenfunctions. A possible temperature behavior of R^e is caused by a change of the internuclear distance with vibrational excitation due to the an-harmonic electronic potential. However, after Born and Oppenheimer [44] the electronic eigenfunctions have a weak dependence on the internuclear distance. The first and second derivatives $\partial\Psi_e/\partial r$ and $\partial^2\Psi_e/\partial r^2$ vanish. Further, a comparison of the dissociation energy D_0'' for the electronic ground state $X^2\Pi_{3/2}$ with the vibrational energy suggests that R^e is constant for all thermally populated vibrational levels. The vibrational energy ω_e of the electronic ground state of BrO is 722.6 cm^{-1} [23]. At 298 K, 96% of the molecules are in the vibrational ground state $v'' = 0$, and 3.3% are in the first excited state $v'' = 1$. We determined D_0'' to 19 372 ± 160 cm^{-1} (see next section). Hence, D_0'' is 93 times larger than the thermal energy at 298 K and 27 times larger than the vibrational energy ω_e. Since only vibrational levels well below the dissociation limit are populated, a very small variation in the internuclear distance and therefore almost no change of R^e may be assumed. In summary, the integral (13) over the UV absorption cross-section of BrO is expected to vary by much less than 1% over the investigated temperature range from 203 to 298 K.

The reaction of halogen atoms with ozone may also produce vibrationally or rotationally excited halogen oxides, disturbing the thermal Boltzmann distribution. On the other hand, the pressure and time scales used in the present experiments were sufficiently large to achieve complete collisional deactivation of these excited states (under these conditions a few 10^8–10^9 collisions per second occur). The time-resolved observation provided no evidence for a relaxation of thermally excited vibrational states. In particular, the strength of the hot bands (2, 1) and (4, 1) did not vary during the observation.

3.2. Vibrational analysis

By a spectroscopic analysis of the TW-FTS spectra, vibrational constants and the dissociation energy for the electronic state $A^2\Pi_{3/2}$ of BrO have been determined. No rotational analysis was carried out, since rotational constants had been derived in the works by Durie and Ramsay [46], Wheeler et al. [28], and Wilmouth et al. [29]. Our study is based on the origins of the vibrational bands in the UV absorption spectrum. The band origins were determined using simulated band spectra. Several ro-vibrational bands for the BrO molecule were synthesized, as described in Refs. [29,47,48]. The bands were simulated because most of them are asymmetric due to the smaller rotational constants in the $A^2\Pi_{3/2}$ state compared to the ground electronic state $X^2\Pi_{3/2}$. This asymmetry is illustrated by Figs. 9 and 10. Rotational constants for the lower electronic state $X^2\Pi_{3/2}$ were taken from Orlando et al. [23], and for the upper state $A^2\Pi_{3/2}$ from Wilmouth et al. [29]. Most vibrational bands are unstructured due to strong pre-dissociation [28,29]. To account for the pre-dissociation broadening, the synthesized bands were convoluted with a Lorentz function. The resulting simulated bands were shifted on the wavenumber axis and scaled to achieve the best agreement with the experimental spectrum. The shifting value then yielded the origin for the respective band.

Table 6
Band origins $\tilde{\nu}_0$ and peak positions $\tilde{\nu}_{peak}$ in vacuum wavenumbers for the observed vibrational bands

(v', v'')	$\tilde{\nu}_0$ (cm^{-1})	$\tilde{\nu}_{peak}$ (cm^{-1})	σ_{peak} ($\times 10^{-17}$ cm^2 per molecule)
(0, 0)	26240 ± 10	26230 ± 10	0.03 ± 0.03
(2, 1)	26495 ± 15	26480 ± 7	0.05 ± 0.03
(1, 0)	26715 ± 4	26675 ± 2	0.09 ± 0.06
(2, 0)	27235 ± 4	27180 ± 2	0.15 ± 0.06
(4, 1)	27471 ± 4	27450 ± 2	0.14 ± 0.06
(3, 0)	27775 ± 3	27735 ± 2	0.29 ± 0.06
(4, 0)	28187 ± 3	28175 ± 2	0.89 ± 0.10
(5, 0)	28683 ± 2	28646 ± 1	0.75 ± 0.10
(6, 0)	29097 ± 3	29066 ± 2	0.97 ± 0.10
(7, 0)	29545 ± 1	29540 ± 1	2.19 ± 0.22
(8, 0)	29981 ± 2	29955 ± 1	1.32 ± 0.14
(9, 0)	30379 ± 2	30346 ± 1	1.24 ± 0.12
(10, 0)	30768 ± 3	30741 ± 2	1.32 ± 0.14
(11, 0)	31156 ± 2	31143 ± 1	1.51 ± 0.16
(12, 0)	31540 ± 2	31527 ± 1	1.30 ± 0.14
(13, 0)	31897 ± 4	31864 ± 2	0.94 ± 0.10
(14, 0)	32233 ± 3	32208 ± 2	0.75 ± 0.08
(15, 0)	32558 ± 2	32530 ± 1	0.65 ± 0.08
(16, 0)	32860 ± 5	32830 ± 3	0.60 ± 0.08
(17, 0)	33160 ± 5	33142 ± 3	0.50 ± 0.08
(18, 0)	33435 ± 7	33410 ± 3	0.47 ± 0.08
(19, 0)	33695 ± 7	33676 ± 3	0.45 ± 0.08
(20, 0)	33936 ± 3	33916 ± 2	0.35 ± 0.08
(21, 0)	34154 ± 3	34140 ± 2	0.27 ± 0.06
(22, 0)	34356 ± 3	34349 ± 2	0.20 ± 0.06
(23, 0)	34530 ± 4	34518 ± 2	0.20 ± 0.06
(24, 0)	34695 ± 10	34655 ± 5	0.17 ± 0.06
(25, 0)	34825 ± 7	34793 ± 3	0.14 ± 0.03
(26, 0)	34935 ± 7	34920 ± 3	0.08 ± 0.03

The fourth column lists the peak cross-sections σ_{peak}. The values $\tilde{\nu}_{peak}$ and σ_{peak} are given for 298 K and a spectral resolution of 3.8 cm^{-1}.

Table 6 lists the experimental band origins and the wavenumber positions of the band peaks for the vibrational progression $(v', 0)$. The observed hot bands (2, 1) and (4, 1) are also included. Further, the peak absorption cross-section for each vibrational band is stated. The spectral resolution is 3.8 cm^{-1}. Both peak wavenumbers and peak cross-sections depend on the spectral resolution. On the other hand, there is no resolution effect on the band origin positions. The wavenumber $\tilde{\nu}_0$ of a band origin in the UV absorption spectrum of BrO can be expressed as

$$\tilde{\nu}_0(v', v'') = T_e + G'(v') - G''(v'') \quad (14)$$

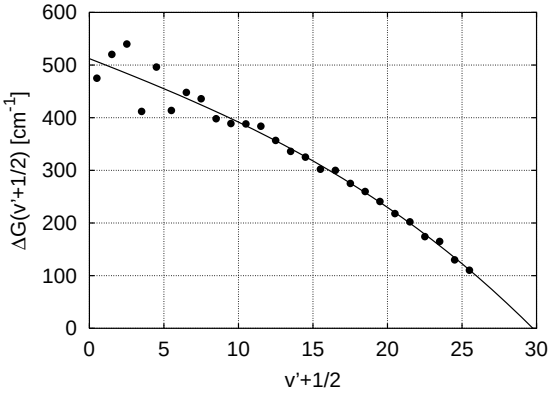

Fig. 12. Birge-Sponer plot for the vibrational progression (v', 0). The energy differences $\Delta G_{v'+1/2}$ between the vibrational bands in the electronic state $A^2\Pi_{3/2}$ are plotted over $v' + 1/2$. The extrapolation is based on a second-order polynomial.

with

$$G(v) = \omega_e(v + \tfrac{1}{2}) - \omega_e x_e(v + \tfrac{1}{2})^2 + \omega_e y_e(v + \tfrac{1}{2})^3 + \cdots \quad (15)$$

Here, T_e is the energy difference between the potential minima of the two involved electronic states, ω_e is the vibrational energy at equilibrium, and v' and v'' are the vibrational quantum numbers in the upper and lower state. The constants x_e and y_e reflect the an-harmonicity of the vibrational potential up to the third order in v. The experimental values for $\tilde{\nu}_0(v', v'')$ are listed in Table 6. The energy differences $\Delta G_{v+1/2} = \tilde{\nu}_0(v' + 1, 0) - \tilde{\nu}_0(v', 0)$ between two adjacent levels of the progression (v', 0) can be used to determine the vibrational constants ω_e, x_e, and y_e for the upper electronic state as well as the dissociation energy. $\Delta G_{v+1/2}$ calculates to

$$\Delta G_{v+1/2} = \omega_e - 2\omega_e x_e + \tfrac{13}{4}\omega_e y_e + v(6\omega_e y_e - 2\omega_e x_e) + v^2 3\omega_e y_e \quad (16)$$

Fig. 12 shows the Birge-Sponer diagram, where the energy separations $\Delta G_{v+1/2}$ are plotted over $v + 1/2$. According to Eq. (16), the energy differences may be approximated by a second-order polynomial. The fitted parabola is also drawn in the figure and extrapolated to the intersections with both axes. For vibrational levels v smaller than 10, the energy differences $\Delta G_{v+1/2}$ are scattered around the average curve. The same observation was reported by Wilmouth et al. [29]. With higher vibrational excitation, the energy differences decrease and the dissociation limit is approached. From the coefficients of the polynomial, the vibrational constants ω_e, x_e, and y_e were derived. The results are listed in Table 7.

The presented vibrational constants for the electronic state $A^2\Pi_{3/2}$ are the first values derived from FTS measurements. Wilmouth et al. [29] recorded high-resolution FT-UV absorption spectra, but did not report vibrational constants. For a comparison to the TW-FTS results, we carried out the vibrational analysis based on the band positions reported in Ref. [29]. Those wavenumber positions represent the band peak locations, which are usually smaller than the origins of asymmetric bands. The latter are independent of temperature and spectral resolution. The difference is illustrated by the value for T_0 in Table 7, which is the energy of the vibrational transition (0, 0). As Table 7 shows, the TW-FTS results are in good agreement with the vibrational constants derived from the band positions reported by Wilmouth et al. The error ranges are also very similar. The covariances are mainly caused by the varying energies at low vibrational excitation, as shown in Fig. 12.

The results from Durie and Ramsay [46] and Barnett et al. [49] are also included in Table 7. Durie and Ramsay did not observe the bands (0, 0) to (3, 0), and therefore based their analysis on a wrong assignment of vibrational quantum numbers. The assignment was later revised by Barnett et al. We re-evaluated the vibrational constants using the band origins reported by Durie and Ramsay [46]. Table 7 shows that these values are in agreement with the TW-FTS observations, but the error ranges are about twice as large. Barnett et al. [49] expressed the band origin positions of the progression (v', 0) by the polynomial $\tilde{\nu}_0 = 26\,237 + 511.3v' - 4.83v'^2 - 0.074v'^3$. The polynomial coefficients were transformed to ω_e, x_e, and y_e, and are also stated in Table 7. Li et al. [50] carried out an ab initio study of the low-lying electronic states of BrO and estimated values for T_e and ω_e. The result for T_e is somewhat higher than the

Table 7
Vibrational constants for the electronic state $A^2\Pi_{3/2}$

	T_e (cm^{-1})	T_0 (cm^{-1})	ω_e (cm^{-1})	x_e ($\times 10^{-3}$)	y_e ($\times 10^{-4}$)
This work	26352 ± 10	26240 ± 10	498 ± 24	6.8 ± 3.4	−2.1 ± 0.8
[29][a]		26228	489 ± 24	5.8 ± 3.5	−2.3 ± 0.8
[46][b]			512 ± 51	8.4 ± 7.3	−1.7 ± 1.6
[49][c]		26241	516.1	9.1	−1.4
[50][d]	27020		478		

The error intervals represent the standard deviation.

[a] The values were determined from the band peak positions as published by Wilmouth et al. [29].

[b] The values were determined by a new analysis using the band origins as stated in Durie and Ramsay [46] with corrected vibrational quantum numbers.

[c] The constants were calculated from the polynomial as given by Barnett et al. [49] for the progression (v', 0).

[d] Ab initio study by Li et al. [50].

Table 8
Experimental results for the dissociation energies of BrO

Reference	D_0 (A ← X)	D_0' ($A^2\Pi_{3/2}$)	D_0'' ($X^2\Pi_{3/2}$)
This work	35240 ± 160 (421.5 ± 1.9)	9000 ± 160 (107.7 ± 1.9)	19372 ± 160 (231.7 ± 1.9)
[29]	35180 ± 140 (420.8 ± 1.7)	8930 ± 140 (106.8 ± 1.7)	19312 ± 140 (231.0 ± 1.7)
[46]	35200 ± 200 (421.0 ± 2.4)	–	19330 ± 200 (231.2 ± 2.4)
[49]	35200 ± 200 (421.0 ± 2.4)	8960 ± 200 (107.2 ± 2.4)	19330 ± 200 (231.2 ± 2.4)

The values are given in cm^{-1} and kJ/mol (in brackets).

TW-FTS value. According to the variation principle, an approximated molecular wave function always yields a higher electronic energy than observed experimentally. Li et al. also obtained a value for the vibrational constant ω_e in the electronic state $A^2\Pi_{3/2}$ ($\omega_e = 478\,cm^{-1}$), which is lower than the experimental results. However, a higher theoretical value for $A^2\Pi$ ($\omega_e = 532\,cm^{-1}$) was yielded, without regarding the spin-orbit coupling. All experimental values as listed in Table 7 are between those two ab initio results for ω_e.

3.3. Dissociation energy

Based on the Birge-Sponer plot in Fig. 12 and a Le Roy-Bernstein extrapolation, the dissociation energy for the upper state $A^2\Pi_{3/2}$ has been determined. The dissociation limit is given by the area under the curve between $v' = 0$ and the intersection of the curve with the v'-axis [48]. The Birge-Sponer extrapolation yielded a dissociation value of $v' = 29.3 \pm 1$ for $\Delta G_{v+1/2} = 0$, and an upper state dissociation energy $D_0' = 8880 \pm 40\,cm^{-1}$. This corresponds to an A ← X dissociation energy $D_0 = 35\,120 \pm 40\,cm^{-1}$. However, the Birge-Sponer extrapolation does not describe very well the vibrational energies for large v near the dissociation limit. Near the dissociation limit of a molecule, the atomic interaction is governed by a long-range potential. According to the Le Roy-Bernstein theory, the function $(\Delta G_{v+1/2})^{(n-2)/(n+2)}$ is linear for large values of v. The constant n is determined by the strongest contribution of the long-range potential. For neutral molecules, n is typically 5 or 6 [48]. The Le Roy-Bernstein extrapolation yielded an A ← X dissociation energy of $D_0 = 35\,400\,cm^{-1}$ for $n = 5$ and $D_0 = 35\,350\,cm^{-1}$ for $n = 6$. Since both methods are approximations, we estimate the A ← X dissociation energy in total to $D_0 = 35\,240 \pm 160\,cm^{-1}$ or 421.5 ± 1.9 kJ/mol. For the upper state dissociation energy we obtained $D_0' = 9000 \pm 160\,cm^{-1}$ or 107.7 ± 1.9 kJ/mol. As mentioned by Durie and Ramsay [46], the lower state dissociation limit D_0'' can be derived by subtracting the energy difference between the excited and the ground-state O atom ($^1D - {}^3P = 15\,868\,cm^{-1}$) from D_0. This yields $D_0'' = 19\,372 \pm 160\,cm^{-1}$ or 231.7 ± 1.9 kJ/mol. The experimental results are listed in Table 8 together with values from previous studies. The TW-FTS results are in good agreement with the other reported values. Wilmouth et al. [29] based their analysis on the band peak positions instead of the band origins. But since this had only little impact on the energy differences of the band positions, the results for the dissociation energies are comparable. Durie and Ramsay [46] did not observe bands at wavenumbers smaller than $28\,000\,cm^{-1}$. For this reason, they did not determine a value for D_0'. This value was later reported by Barnett et al. [49], based on new measurements.

4. Conclusions

New measurements of the UV absorption cross-section of the atmospheric radical BrO have been carried out, using a recently developed technique of time-windowing Fourier transform spectroscopy to observe the bromine-photosensitized decomposition of O_3. The determination of the absolute cross-section was achieved by performing a kinetic analysis of the system. Five different temperatures in the range from 203 to 298 K were studied. This temperature range covers most of the relevant tropospheric and stratospheric temperatures. The integrated UV absorption cross-section of BrO was observed to be almost constant over the entire temperature range studied, in agreement with theoretical considerations. Further, a comparison of the temperature dependence of the cross-sections showed no continuum absorption underlying the structured rotational-vibrational bands of the BrO A–X electronic transitions. This confirms the observation made by Wilmouth et al. [29]. The study of continuum absorption demonstrates some of the advantages of a time-resolved broadband observation method like the TW-FTS. By selecting an appropriate time window with a high concentration of BrO, an optical density between 0.5 and 1 was achieved. This is considerably higher than under static conditions, where BrO concentrations are much lower because of the reactivity of the radical. The higher optical density also reduces any effects arising from baseline drifts.

The absorption cross-sections of BrO determined in this study data provide an interpolation to any particular atmospheric temperature of interest. Moreover, the recorded FTS absorption spectra of BrO have a much higher spectral resolution ($3.8\,cm^{-1}$/0.042 nm) than current remote sensing instruments. We estimate the uncertainty in the wavenumber scaling to be less than $0.6\,cm^{-1}$ (0.007 nm). This enables the generation of appropriate reference spectra for atmospheric observations by spectral convolution with the respective instrumental line shape.

Acknowledgements

This work was supported by the University of Bremen and by the German Space Agency (DLR/Bo. Grant No. 50EP9207). We gratefully acknowledge the technical support by the Bruker Analytik GmbH, Germany.

References

[1] S.C. Wofsy, M.B. McElroy, Y.L. Yung, Geophys. Res. Lett. 2 (1975) 215.
[2] Y.L. Yung, J.P. Pinto, R.T. Watson, J. Atmos. Sci. 37 (1980) 339.
[3] H.K. Roscoe, K. Kreher, U. Friess, Geophys. Res. Lett. 28 (2001) 2911.
[4] M. Martinez, T. Arnold, D. Perner, Ann. Geophys. 17 (1999) 941.
[5] C.T. McElroy, C.A. McLinden, J.C. McConnell, Nature 397 (1999) 338.
[6] F.S. Rowland, M.J. Molina, Rev. Geophys. Space Phys. 78 (1975) 5341.
[7] D.W. Toohey, J.G. Anderson, W.H. Brune, K.R. Chan, Geophys. Res. Lett. 17 (1990) 513.
[8] THESEO (Third European Stratospheric Experiment on Ozone), Stratospheric Ozone Destruction by Bromine, European Commission, Programme Environment and Climate, 1994–1999.
[9] A. Richter, F. Wittrock, M. Eisinger, J.P. Burrows, Geophys. Res. Lett. 25 (1998) 2683.
[10] W.H. Brune, D.W. Toohey, J.G. Anderson, W.L. Starr, J.F. Vedder, E.F. Danielsen, Science 242 (1988) 558.
[11] R. Fitzenberger, H. Bosch, C. Camy-Peyret, M.P. Chipperfield, H. Harder, U. Platt, B.M. Sinnhuber, T. Wagner, K. Pfeilsticker, Geophys. Res. Lett. 27 (2000) 2921.
[12] J.G. Anderson, et al., J. Geophys. Res. 94 (1989) 11480.
[13] M.B. McElroy, Nature 321 (1986) 759.
[14] L.A. Barrie, J.W. Bottenheim, R.C. Schnell, P.J. Crutzen, R.A. Rasmussen, Nature 334 (1988) 138.
[15] J.W. Bottenheim, L.A. Barrie, E. Atlas, L.E. Heidt, H. Niki, R.A. Rasmussen, P.B. Shepson, J. Geophys. Res. 95 (1990) 18555.
[16] M. Hausmann, U. Platt, J. Geophys. Res. 99 (1994) 25399.
[17] F. Wittrock, M. Eisinger, A. Ladstätter-Weißenmayer, A. Richter, J.P. Burrows, Ground based UV/vis measurements of O_3, NO_2, BrO, and OClO over Ny Ålesund (78N), in: Proceedings of XVIII Ozone Symposium, L'Aquila, 1996.
[18] K. Kreher, Spectroscopic measurements of atmospheric OClO, BrO, and NO_2 and their relation to Antarctic ozone depletion, Dissertation, University of Heidelberg, 1996.
[19] K. Chance, Geophys. Res. Lett. 25 (1998) 3335.
[20] A. Wahner, A.R. Ravishankara, S.P. Sander, R.R. Friedl, Chem. Phys. Lett. 152 (1988) 507.
[21] C. Blindauer, V. Rozanov, J.P. Burrows, J. Atmos. Chem. 24 (1996) 1.
[22] R.A. Cox, D.W. Sheppard, M.P. Stevens, J. Photochem. 19 (1982) 189.
[23] J.J. Orlando, J.B. Burkholder, A.M.R.P. Bopegedera, C.J. Howard, J. Mol. Spectrosc. 145 (1991) 278.
[24] M.K. Gilles, A.A. Turnipseed, J.B. Burkholder, A.R. Ravishankara, S. Solomon, J. Phys. Chem. A 101 (1997) 5526.
[25] S.P. Sander, R.T. Watson, J. Phys. Chem. 85 (1981) 4000.
[26] B. Laszlo, R.E. Huie, M.J. Kurylo, A.W. Miziolek, J. Geophys. Res. 102 (1997) 1523.
[27] S.R. Aliwell, M. Van Roozendael, P.V. Johnston, A. Richter, T. Wagner, D.W. Arlander, J.P. Burrows, D.J. Fish, R.L. Jones, K.K. Tornqvist, J.-C. Lambert, K. Pfeilsticker, I. Pundt, J. Geophys. Res. D 107 (2002) 1024.
[28] M.D. Wheeler, S.M. Newman, T. Ishiwata, M. Kawasaki, A.J. Orr-Ewing, Chem. Phys. Lett. 285 (1998) 346.
[29] D.M. Wilmouth, T.F. Hanisco, N.M. Donahue, J.G. Anderson, J. Phys. Chem. 103 (1999) 8935.
[30] R.L. Mauldin, A. Wahner, A.R. Ravishankara, J. Phys. Chem. 97 (1993) 7585.
[31] S. Himmelmann, J. Orphal, H. Bovensmann, A. Richter, A. Ladstätter-Weißenmayer, J.P. Burrows, Chem. Phys. Lett. 251 (1996) 330.
[32] B. Deters, J.P. Burrows, J. Orphal, J. Geophys. Res. 103 (1998) 3563.
[33] O.C. Fleischmann, J. Orphal, J.P. Burrows, J. Photochem. Photobiol. A 157 (2003) 127.
[34] S. Voigt, J. Orphal, K. Bogumil, J.P. Burrows, J. Photochem. Photobiol. A 143 (2001) 1.
[35] D. Maric, J.P. Burrows, G.K. Moortgat, J. Photochem. Photobiol. A 83 (1994) 179.
[36] A.A. Turnipseed, J.W. Birks, J.G. Calvert, J. Phys. Chem. 94 (1990) 7477.
[37] D.M. Rowley, M.H. Harwood, R.A. Freshwater, R.L. Jones, J. Phys. Chem. 100 (1996) 3020.
[38] M.H. Harwood, D.M. Rowley, R.A. Cox, R.L. Jones, J. Phys. Chem. 102 (1998) 1790.
[39] J.B. Burkholder, Int. J. Chem. Kinet. 30 (1997) 571.
[40] United Kingdom Atomic Energy Authority (UK AEA), FACSIMILE RELEASE H023 DATE 16/09/92 VERSION 101010, 1991.
[41] W.B. DeMore, S.P. Sander, C.J. Howard, A.R. Ravishankara, D.M. Golden, C.E. Kolb, R.F. Hampson, M.J. Kurylo, M.J. Molina, Chemical Kinetics and Photochemical Data for use in Stratospheric modeling, Jet Propulsion Laboratory, Pasadena, CA, 1997.
[42] U. Platt, D. Perner, J. Geophys. Res. 85 (1980) 7453.
[43] R.S. Mulliken, J. Chem. Phys. 7 (1939) 20.
[44] M. Born, R. Oppenheimer, Ann. Phys. 84 (1927) 457.
[45] A.R.W. McKellar, J. Mol. Spectrosc. 86 (1981) 43.
[46] R.A. Durie, D.A. Ramsay, Can. J. Phys. 36 (1958) 35.
[47] G. Herzberg, Spectra of Diatomic Molecules, Van Nostrand Reinhold, New York, 1950.
[48] P.F. Bernath, Spectra of Atoms and Molecules, Oxford University Press, Oxford, 1995.
[49] M. Barnett, E.A. Cohen, D.A. Ramsay, Can. J. Phys. 59 (1981) 1908.
[50] Y. Li, J.S. Francisco, K.A. Peterson, J. Chem. Phys. 113 (2000) 8556.